Journal of Experimental Botany, Vol. 61, No. 12, pp. 3355–3370, 2010
doi:10.1093/jxb/erq157 Advance Access publication 7 June, 2010

Journal of Experimental Botany
www.jxb.oxfordjournals.org

RESEARCH PAPER

The differential spatial distribution of secondary metabolites in *Arabidopsis* leaves reacting hypersensitively to *Pseudomonas syringae* pv. *tomato* is dependent on the oxidative burst

Clara Simon[1], Mathilde Langlois-Meurinne[1], Floriant Bellvert[1,2,3,4], Marie Garmier[1], Laure Didierlaurent[1], Kamal Massoud[1], Sejir Chaouch[1], Arul Marie[5], Bernard Bodo[5], Serge Kauffmann[6], Graham Noctor[1] and Patrick Saindrenan[1,*]

[1] Institut de Biologie des Plantes, CNRS-Université Paris-Sud 11, UMR 8618, Bâtiment 630, 91405 Orsay Cedex, France
[2] Centre d'Etudes des Substances Naturelles (CESN), Université de Lyon Villeurbanne, France
[3] CNRS, UMR 5557 Ecologie Microbienne, Villeurbanne, France
[4] Université de Lyon, Lyon 1, Villeurbanne, France
[5] Muséum National d'Histoire Naturelle, CNRS-MNHN, UMR 5154, 63 rue Buffon, F-75005 Paris, France
[6] Institut de Biologie Moléculaire des Plantes, CNRS, UPR 2357, 12 rue du Général Zimmer, F-67084 Strasbourg, France

* To whom correspondence should be addressed: E-mail: patrick.saindrenan@u-psud.fr

Received 22 March 2010; Revised 10 May 2010; Accepted 13 May 2010

Abstract

Secondary metabolites (SMs) play key roles in pathogen responses, although knowledge of their precise functions is limited by insufficient characterization of their spatial response. The present study addressed this issue in *Arabidopsis* leaves by non-targeted and targeted metabolite profiling of *Pseudomonas syringae* pv. *tomato* (*Pst-AvrRpm1*) infected and adjacent uninfected leaf tissues. While overlap was observed between infected and uninfected areas, the non-targeted metabolite profiles of these regions differed quantitatively and clustering analysis underscores a differential distribution of SMs within distinct metabolic pathways. Targeted metabolite profiling revealed that infected tissues accumulate more salicylic acid and the characteristic phytoalexin of *Arabidopsis*, camalexin, than uninfected adjacent areas. On the contrary, the antioxidant coumarin derivative, scopoletin, was induced in infected tissues while its glucoside scopolin predominated in adjacent tissues. To elucidate the still unclear relationship between the accumulation of SMs and reactive oxygen species (ROS) accumulation and signalling, a catalase-deficient line (*cat2*) in which ROS signalling is up-regulated, was used. Metabolic analysis of *cat2* suggests that some SMs have important interactions with ROS in redox homeostasis during the hypersensitive response to *Pst-AvrRpm1*. Overall, the study demonstrates that ROS availability influences both the amount and the pattern of infection-induced SM accumulation.

Key words: *Arabidopsis thaliana*, metabolite profiling, oxidative burst, plant defence, *Pseudomonas syringae* pv. *tomato*, secondary metabolites.

Introduction

Plant resistance to pathogen infection is often associated with the development of the hypersensitive response (HR) that results in a layer of dead cells that restricts pathogen spread (Mur *et al.*, 2008). During the HR, biosynthetic pathways are highly activated, especially those leading to the production of secondary metabolites (SMs) (Dixon, 2001). The stimulation of the indolic pathway is one of the major metabolic alterations occuring in *Arabidopsis*

(*Arabidopsis thaliana*) leaves reacting hypersensitively to the avirulent bacteria *Pseudomonas syringae* pv. *tomato* carrying the *AvrRpm1* gene (*Pst-AvrRpm1*) (Hagemeier *et al.*, 2001).

SMs perform multiple functions in plants associated with ecological roles in defence against biotic and abiotic stresses. These functions include roles in UV-B protection (Winkel-Sherley, 2002), lignification (Coleman *et al.*, 2008), herbivore protection and defence against pathogens (Dixon, 2001; Halkier and Gershenzon, 2006; Bednarek *et al.*, 2009; Clay *et al.*, 2009). However, it is becoming apparent that SMs also play roles in endogenous plant signalling networks. Salicylic acid (SA) is a major signalling molecule involved in the induction of defence responses against pathogens (Loake and Grant, 2007). Sclareol, a diterpene, was shown to be involved in a wound- and tobacco mosaic virus (TMV)-activated signal transduction in tobacco (Seo *et al.*, 2003). Moreover, new internal roles for SMs as cellular protectants have recently been demonstrated. The coumarin derivative scopoletin and some monoterpenes were shown to be associated, respectively, with protection against reactive oxygen species (ROS) produced during the HR to TMV in tobacco (Chong *et al.*, 2002; Gachon *et al.*, 2004) and with exposure of *Quercus ilex* leaves to ozone (Loreto *et al.*, 2004). To date, approximately 200 SMs has been identified in *Arabidopsis*, but considering the huge gene families encoding enzymes participating in secondary metabolism, it is likely that a large number of compounds and their corresponding functions await discovery (D'Auria and Gershenzon, 2005). The question of whether all these compounds play roles in plant protection is still a matter of debate. Reverse genetics studies provide some evidence of the involvement of SMs in resistance against pathogens. For example, the *Arabidopsis pad3* mutant is unable to produce the indole phytoalexin camalexin (3-thiazol-2′-yl-indole) in response to pathogens such as the avirulent *P. syringae* (Glazebrook and Ausubel, 1994) and *Alternaria brassisicola* (Thomma *et al.*, 1999). Although the *pad3* mutant exhibited enhanced susceptibility to the fungus, it allowed the same *in planta* growth of the bacterium as the wild-type plant, suggesting that camalexin did not provide resistance in this particular interaction (Glazebrook and Ausubel, 1994).

One important factor in ascertaining the significance of SMs during the HR is qualitative and quantitative knowledge of their spatial distribution in challenged tissues. The reason is because HR involves both cells committed to die at the infection site and metabolically active cells in the lesion periphery. Thus, analyses at the level of a whole organ would not give a clear picture of the metabolic events occuring in the HR. Pioneering works of Hahn *et al.* (1985) indicated that glyceollin I, the major phytoalexin of soybean roots, accumulated at the site of infection with the incompatible race of *Phytophthora megasperma*, thus providing sufficient inhibitory activity, whereas its concentration dropped sharply at the leading edge of the infection. SA at low doses was shown to prime the activation of defence responses and to control the spread of HR immediately around the lesions (Alvarez, 2000). Careful work using the oomycete elicitin from *Phytophthora megasperma* to elicit HR-like cell death has shown a strong association between cell death and the subsequent activation of specific defences in neighbouring tissues, and particularly the accumulation of SMs (Dorey *et al.*, 1997; Costet *et al.*, 1999). On the whole, it appears that the perception by plant cells of a pathogenic signal inducing an HR leads to cell death at the site of infection, and to the generation of signal(s) triggering strong defence responses in the surrounding cells, particularly activation of secondary metabolism pathways (Costet *et al.*, 2002).

Spatial distribution of SMs in tissues undergoing HR is often associated with an oxidative burst characterized by the production of ROS including the superoxide anion ($O_2^{\cdot-}$), hydrogen peroxide (H_2O_2), and the induction of cellular protectants like glutathione-*S*-transferases that block oxidant-mediated cell death in surrounding cells (Lamb and Dixon, 1997). One of the major enzymatic systems for the removal of H_2O_2 in plant cells is catalase (CAT) (Foyer *et al.*, 2009). In tobacco leaves reacting hypersensitively to a glycoprotein elicitor, induction of a class II catalase gene (*CAT2* in tobacco) was shown to occur in tissues bordering the infiltrated area (Dorey *et al.*, 1998). Thus, the distribution of SMs appears to match with the induction of protective genes against the oxidative burst.

In this study, a simple model system was designed to address the question of the differential spatial distribution of SMs in relation to their potential functions during the HR of *Arabidopsis* leaves to *Pst-AvrRpm1*. Non-targeted and targeted metabolite profiling demonstrate a spatial organization of SMs at, and in the vicinity of, the infection site where a differential accumulation within distinct metabolic pathways is observed. Because SMs have important interactions with ROS (Chong *et al.*, 1999; Baker *et al.*, 2002; Loreto *et al.*, 2004), their distribution was also examined in leaves of catalase2-deficient plants (*cat2*) (Queval *et al.*, 2007) infected with *Pst-AvrRpm1*. The results indicate that ROS availability influences both the amount and the pattern of *Pst-AvrRpm1*-induced SM accumulation.

Materials and methods

Biological materials, plant treatments, and sampling

Arabidopsis (*Arabidopsis thaliana*) ecotype Columbia (Col-0) was used throughout this study. The catalase-deficient mutant *cat2* in the Col-0 background was described by Queval *et al.* (2007). Plants were grown in soil under a 8/16 h light/dark photoperiod at 150 µE m^{-2} s^{-1} of light intensity, at 20/18 °C day/night and 65/65% day/night relative humidity. The avirulent strain *Pseudomonas syringae* pv. *tomato* DC3000 carrying the avirulence gene *AvrRpm1* (*Pst-AvrRpm1*) was obtained from J Glazebrook (University of Minnesota, St Paul, USA). Six to seven-week-old plants were used for the *Pst-AvrRpm1* inoculation of half leaves at a concentration of 10^7 cfu ml^{-1} (A_{600}=0.01) as described by Langlois-Meurinne *et al.* (2005), except for the the infiltration of mock-infiltrated leaves with 10 mM $MgCl_2$. The infiltrated half leaves and the adjacent uninfiltrated half leaves of five to eight different plants were harvested, pooled, weighed (about 150 mg FW) at each time point and frozen in liquid nitrogen.

Cell death and reactive oxygen species detection

Cell death was detected by trypan blue staining as described by Bowling *et al.* (1997). Accumulation of ROS was detected using the 3,3'-diaminobenzidine (DAB) staining (Dutilleul *et al.*, 2003). ROS were visualized as a brown coloration at the site of DAB polymerization. Staining intensities were quantified using ImageJ software (http://rsb.info.nih.gov/ij/index.html).

Pst-AvrRpm1 *detection*

Verification of the presence or absence of bacteria in leaves was performed by PCR on *AvrRpm1* gene in extracted half leaf DNA at 24 h post-inoculation (hpi). Samples were ground to a fine powder for 1 min at 30 Hz in a Retsch MM300 grinder (F-Kurt Retsch GmbH & Co., Haan, Germany), homogenized for 5 min in 1.2 ml buffer (200 mM TRIS pH 7.5, 250 mM NaCl, 25 mM EDTA, 0.5% SDS), and centrifuged for 10 min at 16 000 *g* at room temperature (RT). Volumes of 0.7 ml of the resulting supernatants were briefly homogenized in 0.7 ml isopropanol and samples were centrifuged for 15 min at 16 000 *g*. Pellets were washed with 1 ml of 70% ethanol, vacuum-dried, and resuspended in 100 µl of sterile water. Extracted DNA (100 ng) was subjected to a PCR program including a hot start at 94 °C for 2 min followed by 35 cycles of 30 s at 94 °C, 45 s at 63 °C and 1 min at 72 °C. The 680 bp PCR product amplified from the *AvrRpm1* sequence was generated using the following primer set: *AvrRpm1* F: 5′-GGGATCCACCA-TGGGCTGTGTATCGAGC-3′ and *AvrRpm1* R: 5′-GACGCG-TATCTTAAAAGTCATCTTC-3′.

Non-targeted metabolite profiling

Soluble metabolites were extracted and analysed as described by Hagemeier *et al.* (2001) except for corrections for losses performed with the addition of [^{14}C]SA (50 Bq, 2 GBq mmol^{-1}, NEN, UK) to each sample. Samples (100 µl) were subjected to high performance liquid chromatography (HPLC) analysis on a Symmetry 5 µm C-18 column (250×4.6 mm, Waters corporation, Milford, USA) with 0.01% aqueous TFA as solvent A and acetonitrile with 0.01% TFA as solvent B, at a flow rate of 1 ml min^{-1}. Peak detection was performed with a Photodiode Array Detector (PAD) (200–600 nm) as part of the Waters system (Waters Corporation, Milford, USA). HPLC chromatograms were analysed at 273 nm using Empower Pro Software (Waters Corporation, Milford, USA). A manual alignment was performed on the 100 detectable peaks for all HPLC chromatograms. Among the peaks, a set of 44 relevant peaks was selected according to their highly reproducible patterns among all the samples of two independent experiments. Relative abundance of metabolites was estimated on the peak area at 273 nm. Peak purity was checked by acquisition of spectra (λ=200–400 nm) and use of the angle theory of purity peak algorithm of the Empower Pro Software. Metabolites were identified by Mass Spectrometry (MS) and by using KNApSAcK (http://kanaya.aist-nara.ac.jp/KNApSAcK/), Metlin (http://metlin.scripps.edu/) databases, and available published data. When standards were available, identification of metabolites was confirmed by comparison of their retention times (Rt) and UV spectra with those of their corresponding standards.

Salicylic acid, camalexin, and scopoletin quantification

SA, camalexin, and scopoletin were analysed at 0, 10, and 24 hpi. SA, camalexin, and scopoletin were extracted as described by Baillieul *et al.* (1995) with the following modifications. [^{14}C]SA (50 Bq, 2 GBq mmol^{-1}) was added to each sample to correct for losses. Samples were dried in a SC 110A Speed-Vac (Savant Instrument Inc., New York, USA). One-half of the dried samples was kept dried in darkness at RT to analyse camalexin and free forms of SA and scopoletin. The other dried samples were submitted to acidic hydrolysis in order to determine total SA and scopoletin (free plus conjugated forms). The sample extraction and HPLC analysis were achieved according to Baillieul *et al.* (1995) using fluorescence detection. Purity of peaks and corrections for losses were performed as described above. SA, camalexin, and scopoletin were quantified based on a comparison of their peak areas with those of their respective standards. The camalexin standard was a gift of A Bucchala (Fribourg University, Switzerland). SA, camalexin, and scopoletin were identified by comparison of their Rt and UV spectra with those of their corresponding standards. Scopoletin identification was confirmed by LC-MS at the Institut de Biologie Moléculaire des Plantes (Strasbourg, France).

Metabolite identification by MS, MS-MS and LC-MS

Metabolites of interest were collected and subjected to MS and MS-MS analysis. The solvent was evaporated at RT using a Speed-Vac. Mass spectra were acquired using a Quadrupole-Time of flight (Q-TOF) hybrid mass spectrometer (*pulsar i*, Applied Biosystems, France) equipped with an electrospray ionization source (ESI). Acetonitrile and 1% formic acid (1:1) were pumped to the electrospray source, at a flow rate of 20 µl min^{-1}, using two micro-HPLC pumps (series 200 LC pumps, Perkin Elmer, USA). The samples were dissolved in 10 µl of 100% methanol and about 1 µl was manually injected. The ionspray and declustering potential were 5200 V and 30 V, respectively. All the mass spectra were recorded in the positive ion mode. For MS-MS experiments, the parent ions were selected using a unit resolution window and the collision energy varied between 20 V and 40 V.

Additional sample analyses were performed on an Agilent 1200 series HPLC equipped with a degasser (G132A), a quaternary pump module (G1311A), an automatic sampler (G1329A) and a PAD (model G1315B). Software used for analysis and integrations was ChemStation for LC 3D Systems Rev. B.01.03. Separations were carried out using a Symmetry 5 µm C-18 column (250×4.6 mm, Waters Corporation, Milford, USA). Elution was conducted by an increase of acetonitrile (supplemented with 0.05% of TFA) into water (with 0.05% of TFA) at a flow rate of 0.8 ml min^{-1}. UV-visible spectra were recorded between 200 and 800 nm and chromatograms used for analyses were recorded at 273 nm. Injection volumes were 50 µl. The HPLC system was interfaced with an HP Mass Spectrometer Detector (MSD) 1100 series allowing the same chromatographic conditions as those used for HPLC-PAD analysis. The operating conditions for MS with an ESI interface were: gas temperature 350 °C at a flow rate of 10 ml min^{-1}, nebulizer pressure 30 psi quadripole temperature 30 °C, capillary voltage 3500 V and fragmentor 100. Full scan spectra from *m/z* 100 to 1500 in both positive and negative ion modes were obtained.

Data analysis

ANOVA was performed for each metabolite on raw data of peak areas of two series of triplicates of two independent experiments using StatBox 6.40 software (Grimmersoft, Issy les Moulineaux, France). Principal Component Analysis (PCA) was performed on normalized $\log_{10}$-transformed data of 44 peak areas for 59 samples from two independent experiments, using StatBox 6.40 software. Samples and metabolites were clustered according to their relative induction or repression compared to the median value of all peak areas. Data of 44 peak areas for 59 samples were normalized and subjected to average linkage hierarchical clustering with the Pearson correlation coefficient as a distance measure with the MeV 4.0 software (Saeed *et al.*, 2003). The reliability of sample and metabolite clusters was assessed with experiment bootstrapping (1000 replications).

RT-PCR analysis

Total RNA were extracted from ground, frozen material using Extract All mix (Eurobio) according to the manufacturer's

intructions. Samples were subjected to RNase-free DNase I treatment (DNA-free™ kit, Ambion®, Applied Biosystems) for 30 min. Total RNA were loaded on a 1% agarose gel to check their integrity, and the amount of total RNA was determined spectrophotometrically. Three micrograms of total RNA were reverse transcribed using the SuperScript II™ First-Strand cDNA synthesis system (Invitrogen Life Technologies) according to the manufacturer's instructions. PCR was performed using the GoTaq® Flexi DNA Polymerase (Promega) in a 25 µl reaction mixture containing 1.25 U DNA polymerase, 5 nmol of each dNTP, 1× Green Flexi Buffer, and 10 pmol of each gene-specific primer. The gene-specific primers were used as follows: *ICS1-F* (5′-TTGGTGGCGAGGAGAGTG-3′) and *ICS1-R* (5′-CTTCCAGCTACTATCCCTGTCC-3′) for *ISOCHORISMATE SYNTHASE1* (At1g74710; Tm=60 °C); *PAD3-F* (5′-CGTTTATGCGATGGGTCGTG-3′) and *PAD3-R* (5′-GTGGTGAAGAACTTGAAAGAAGGC-3′) for *PHYTOALEXIN DEFICIENT3* (At3g26830; Tm=55 °C); *F6'H1-F* (5′-TACTACCCCATCTGCCCTAATCCG-3′) and *F6'H1-R* (5′-TCTTTCCATCGTGTGCCTTCC-3′) for *FERULOYL-CoA 6'HYDROXYLASE* (At3g13610; Tm=56.5 °C); *ACT2-F* (5′-GTGAAGGCTGGATTTGCAGGA-3′) and *ACT2-R* (5′-AACCTCCGATCCAGACACTGT-3′) for *ACTIN2* (At3g18780; Tm=60 °C). PCR reactions were run on a 2720 Thermal Cycler (Applied Biosystems). After a 2 min denaturation step at 94 °C, samples were run for 25 cycles of 30 s at 94 °C, 30 s at indicated Tm and 30 s (for *PAD3*, *F6'H1*, *ICS1*) or 45 s (for *ACTIN2*) of elongation at 72 °C. PCR products were separated by agarose gel electrophoresis and stained with ethidium bromide.

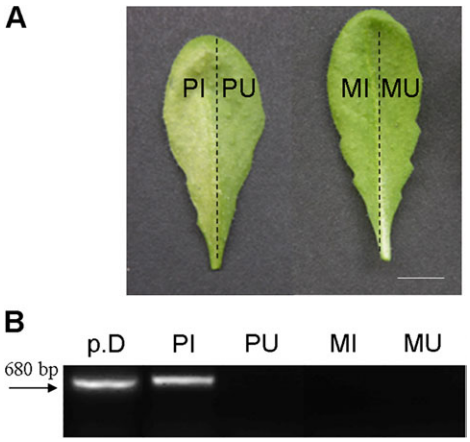

Fig. 1. Detection of *Pst-AvrRpm1* bacteria in *Arabidopsis* leaves. (A) Representative *Arabidopsis* leaves 48 h after infiltration of the left half leaves with *Pst-AvrRpm1* (10^7 cfu ml^{-1}) or $MgCl_2$. Bar=8 mm. (B) PCR amplification of *AvrRpm1* plasmidic gene. PCR amplification was performed using the following templates: p.D, purified bacterial DNA; PI, DNA isolated from *Pst-AvrRpm1* infiltrated tissues; PU, DNA isolated from uninfiltrated part of *Pst-AvrRpm1* treated leaves; MI, DNA from the $MgCl_2$ (mock) infiltrated tissues; MU, DNA from the uninfiltrated part of mock-treated leaves. Tissues were collected 24 h after treatments for DNA extraction. Amplification product size=680 bp (indicated by the arrow). The experiment was repeated twice with identical results.

Results

Metabolite profiling indicates quantitative rather than qualitative differences in secondary metabolite accumulation in Pst-AvrRpm1*-infected and -uninfected leaf tissues*

The metabolite profiling method described by Hagemeier *et al.* (2001) was used among the profiling schemes developed in recent years for *Arabidopsis* leaves infected with *Pseudomonas* (Hagemeier *et al.*, 2001; Tan *et al.*, 2003; Schmelz *et al.*, 2004). Corresponding halves of matching *Arabidopsis* leaves were inoculated with *Pst-AvrRpm1* or mock-infiltrated with $MgCl_2$ and non-targeted metabolite profiling was performed on the *Pseudomonas*-infiltrated (PI) and *Pseudomonas*-uninfiltrated (PU) halves of each leaf, on the mock-infiltrated (MI) and mock-uninfiltrated (MU) adjacent half-part of leaves (Fig. 1A). Leaves of untreated plants were analysed as an additional control. HR symptoms became clearly visible 48 h post-inoculation (hpi) (Fig. 1A) and remained limited to the bacteria-infiltrated tissues. PU tissues were shown to remain devoid of bacteria at 48 hpi as confirmed by the absence of amplified *Pst-AvrRpm1* DNA (Fig. 1B). Soluble SMs were extracted and samples were subjected to reverse-phase HPLC coupled to UV-PDA detection. Peak purity was checked by acquisition of spectra (λ=200–400 nm) and use of multivariate analysis. The most complex profiles were obtained at 273 nm, hence further profiling and data acquisition were performed at this wavelength. Figure 2 shows the profiles of metabolites extracted from PI, PU, and MI tissues. More than 100 peaks were detected among which a subset of 44 peaks was selected by their purity and highly reproducible patterns between two independent experiments. Among these 44 peaks, 15 of the most abundant detectable compounds were analysed either by electrospray ionization ion-trap mass spectrometry detection (HPLC/ESI-QTOF-MS) or by HPLC/PDA/ESI-MS. Nine compounds have been identified unequivocally (see Supplementary Table S1 at JXB on line): adenosine (1); phenylalanine (Phe) (2); tryptophan (Trp) (5); two indolic derivatives, indole-3-carboxylic acid β-D-glucopyranosyl ester (8) and camalexin (14); three flavonols, kaempferol 3-*O*-[6″-*O*-rhamnosyl-glucoside]-7-*O*-rhamnoside (7), kaempferol 3-*O*-glucoside 7-*O*-rhamnoside (10), and kaempferol 3-*O*-rhamnoside 7-*O*-rhamnoside (11); and a sinapoyl ester, sinapoyl malate (12). Most of these compounds have been previously described in *Arabidopsis* infected leaves (Hagemeier *et al.*, 2001) with the exception of Phe and adenosine. Metabolites (3) and (9) were putatively annotated as a benzoic acid derivative, 4-hydroxybenzoylcholine and an indolic derivative, dihydrocamalexic acid, respectively. Compound (13) was proved to be an indole-3-carboxylic acid conjugated to an unidentified residue.

Relative variation in metabolite abundance among PI, PU, MI, and MU tissues was determined. No appreciable differences between profiles of MI and MU tissue samples could be observed excluding any treatment effect (see Supplementary Fig. S1 at *JXB* online), whereas profiles of PI and PU tissue samples revealed mostly quantitative differences (Fig. 3). The accumulation of 17 compounds was significatively enhanced in PI tissues compared with PU tissues, for example, compounds (2), (5), (8), (13), and (14),

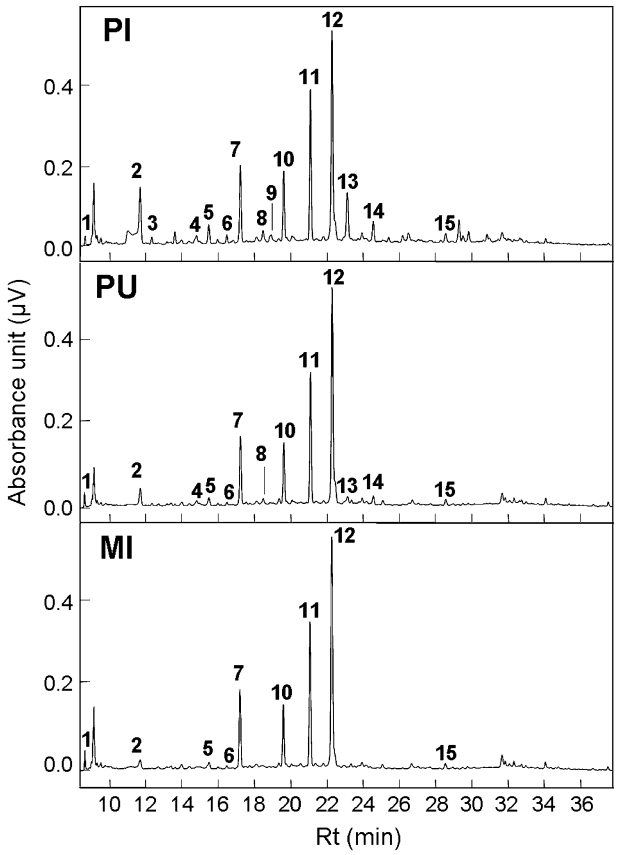

Fig. 2. Metabolite profiling of soluble secondary metabolites from *Pst-AvrRpm1*-infected tissues (PI) at an inoculum density of 10^7 cfu ml^{-1}, the uninfected adjacent part of leaves (PU), and mock-infiltrated tissues (MI) 24 hpi. HPLC profiles were obtained from aqueous methanolic extracts. Chromatograms were analysed by UV detection at 273 nm. Peak numbering corresponds to (1) adenosine, Rt 8.56 min; (2) phenylalanine, Rt 11.63 min; (3) 4-hydroxybenzoylcholine, Rt 12.28 min; (4) compound not determined, Rt 14.85; (5) tryptophan, Rt 15.40 min; (6) compound not determined, Rt 16.39; (7) kaempferol 3-*O*-[6″-*O*-(rhamnosyl) glucoside] 7-*O*-rhamnoside, Rt 17.15 min; (8) indole-3-carboxylic acid β-D-glucopyranosyl ester, Rt 18.42 min; (9) dihydrocamalexic acid, Rt 18.90 min; (10) kaempferol 3-*O*-glucoside 7-*O*-rhamnoside, Rt 19.53 min; (11) kaempferol 3-*O*-rhamnoside 7-*O*-rhamnoside, Rt 21.01 min; (12) sinapoyl malate, Rt 22.22 min; (13) indolic derivative, Rt 23.06 min; (14) camalexin, Rt 24.49 min; (15) compound not determined, Rt 28.49 min.

four of them deriving from the indolic pathway. Conversely, the levels of 14 compounds were diminished in PI tissues compared with PU tissues, for example, compound (12). No change was observed for 10 compounds such as compounds (7), (10), and (11) which belong to flavonol derivatives. Few qualitative differences between PI and PU were observed. The unknown compounds with Rt 29.15 min (λ_{max} 242 nm, 313 nm), Rt 30.87 min (λ_{max} 250 nm, 280 nm), and Rt 31.36 min (λ_{max} undetermined) were only detected in PI tissues. Unfortunately, insufficient material corresponding to these compounds in PI tissues was collected to allow further chemical characterization. Noteworthy, none of the compounds present in PU tissues was absent in PI tissues. All these results suggest that spatial differences in SM accumulation between PI and PU tissues are largely quantitative rather than qualitative.

Organization of secondary metabolites within leaf areas and metabolic pathways

Hierarchical cluster analysis (HCA) was used to cluster the metabolites and tissue samples according to their relative abundance and their distribution pattern. HCA was realized on a matrix of 44 peak areas within 59 samples. Due to the nature of the data under analysis which are subject to biological variation, it was empirically determined that bootstrap values over 50% could be considered as significant (Gachon *et al.*, 2005). High bootstrap values (100%) differentiated samples into three principal clusters: PI tissues 10 hpi, PI tissues 24 hpi, and the other tissues (Fig. 4). The untreated leaves differed from the PU, MI, and MU tissues with a bootstrap value of 60–70%. Principal component analysis (PCA) confirmed and extended the results of HCA (see Supplementary Fig. S2 at *JXB* online). Besides the aforementioned clusters revealed with HCA, PCA clearly discriminated PI samples from PU samples, especially at 24 hpi, and PU samples from MI and MU samples at 10 and 24 hpi on the score plots (see Supplementary Fig. S2 at *JXB* online). Moreover, HCA revealed four major clusters within metabolites (Fig. 4). Clusters A and B differed from clusters C and D with a bootstrap value of 100%. Clusters A and B, which differed with a bootstrap value of 65%, regrouped SMs mainly induced in PI tissues. Clusters C and D exhibited compounds whose accumulation was not induced or repressed in PI tissues. Application of PCA algorithms to the 44 metabolites (loading plots) showed that metabolite clusters are partially grouped within clusters corresponding to those described in HCA (see Supplementary Fig. S3 at *JXB* online). However, PCA did not segregate metabolites belonging to clusters A and B (Fig. 4), because most of the metabolites induced at 10 hpi in cluster B were also induced at 24 hpi (*e.g.* all metabolites in cluster A). A comparison of score plots (see Supplementary Fig. S2 at *JXB* online) and loading plots (see Supplementary Fig. S3 at *JXB* online) revealed that metabolites of clusters A and B, cluster C, and cluster D made a large contribution to PI tissue segregation (10 and 24 hpi), from untreated leaves, and from PU tissues (10 and 24 hpi), respectively. With the exception of 4-hydroxybenzoylcholine (4-OHBenCh), SMs belonging to cluster A (Fig. 4) included the indolic compounds previously described (see Supplementary Table S1 at *JXB* online). For example, indole-3-carboxylic acid β-D-glucopyranosyl ester (I3CAGlc) and the indolic derivative with an Rt of 23.06 min increased gradually from 10 h to 24 h after *Pst-AvrRpm1* inoculation (Fig. 5A). Interestingly, the Trp level decreased in PI tissues at 10 hpi suggesting its immediate use in defence-orientated biosynthetic pathways, whereas it accumulated in the same tissues at 24 hpi, probably as a pool of precursor for other

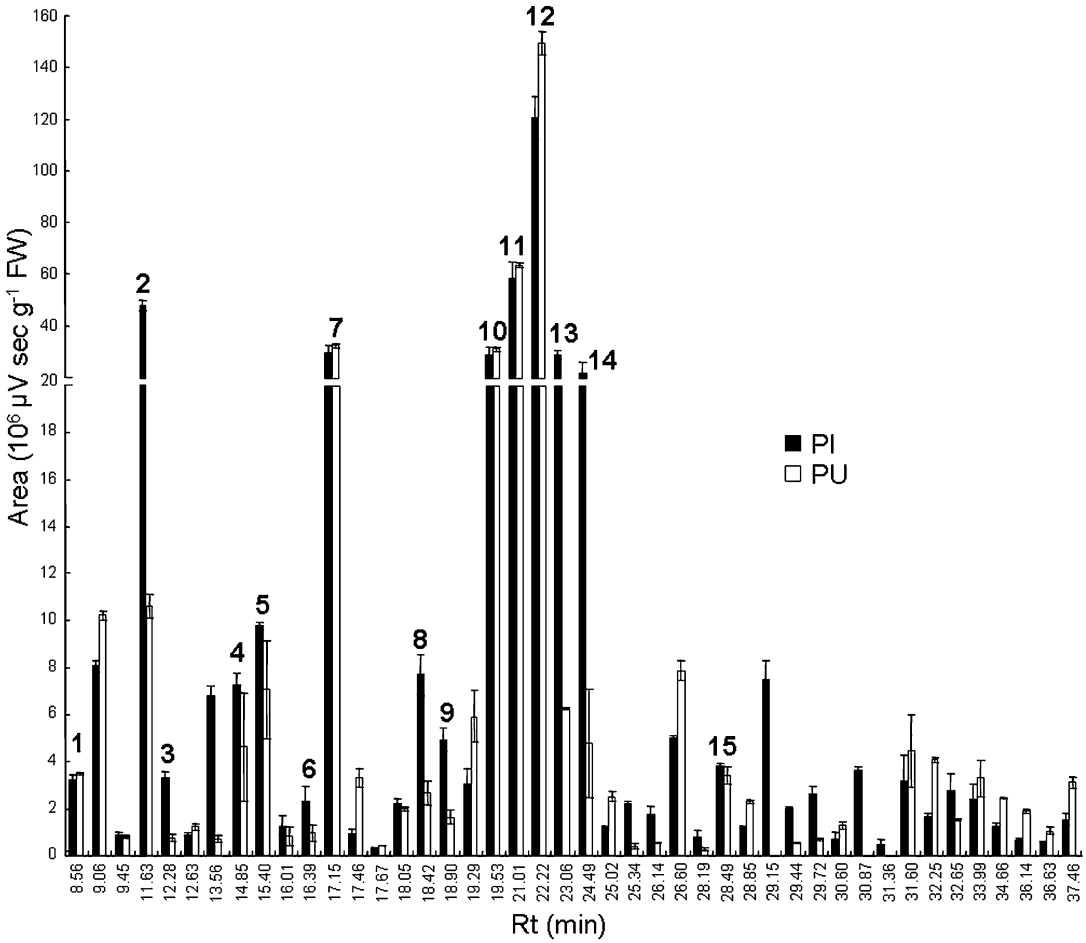

Fig. 3. Relative abundance of 44 secondary metabolites from *Pst-AvrRpm1*-infected tissues (PI, black bars) and uninfected adjacent part of leaves (PU, white bars). Levels of secondary metabolites were quantified 24 hpi at 273 nm. Values correspond to the mean (±SE) of six replicates from two independent experiments. Peak numbering corresponds to the metabolites described in Fig. 2.

metabolic pathways or protein biosynthesis. Camalexin was highly induced in PI tissues compared with PU tissues (Fig. 5A). Moreover, all the indolic compounds within cluster A were more accumulated in PI tissues than in PU tissues. The accumulation of SMs belonging to cluster B was induced earlier than that of cluster A and was observed mainly in PI tissues (Fig. 4). The sole compound identified in cluster B was Phe which accumulated early in PI tissues after infection and whose level remained high 24 hpi (Fig. 5B). The unknown compound with an Rt of 32.65 min showed a striking induction pattern. It was the only compound in this cluster which exhibited a higher level at 10 hpi than at 24 hpi with *Pst-AvrRpm1* (Fig. 5B), suggesting an early role for this compound in PI tissues. The behaviour of SMs in clusters C and D differed dramatically from those observed in clusters A and B (Figs 4, 5). Levels of SMs in cluster C were either not affected or decreased during the infection. Three kaempferol derivatives (kaempferol 1, 2, and 3) and sinapoyl malate belonged to this cluster (Fig. 4). The three flavonols were grouped together with a bootstrap value close to 100% (Fig. 4). This example confirmed that metabolite association supported by high bootstap values can be interpreted as biologically relevant. Kaempferol 1 (kaempferol 3-*O*-[6″-*O*-rhamnosyl-glucoside]-7-*O*-rhamnoside) exhibited a steady-state level in both PI and PU tissues after infection (Fig. 5C). Sinapoyl malate content of PI tissues decreased by 15%, but not significantly, 24 hpi with *Pst-AvrRpm1*. On the contrary, levels of the unknown compound with Rt 25.02 min decreased significantly in PI tissues, 10 hpi and 24 hpi (Fig. 5C). None of the SMs detected in cluster C was affected in PU tissues. Cluster D differed from cluster C with a bootstrap value ranging from 60% to 70% (Fig. 4). The eight unknown compounds of this cluster showed particular trends. While their levels decreased in PI tissues (Fig. 4), more interestingly they increased in PU tissues at 24 hpi, as shown for the unknown compound with an Rt of 37.46 min (Fig. 5D). As such, cluster D embraced compounds specifically induced in PU tissues, although to low levels, with tendencies to decrease in PI tissues. However, none of these compounds has been yet identified.

Altogether, these data demonstrate a spatial organization of SMs at, and close to the site of infection, and underscore a differential distribution of these SMs within distinct metabolic pathways.

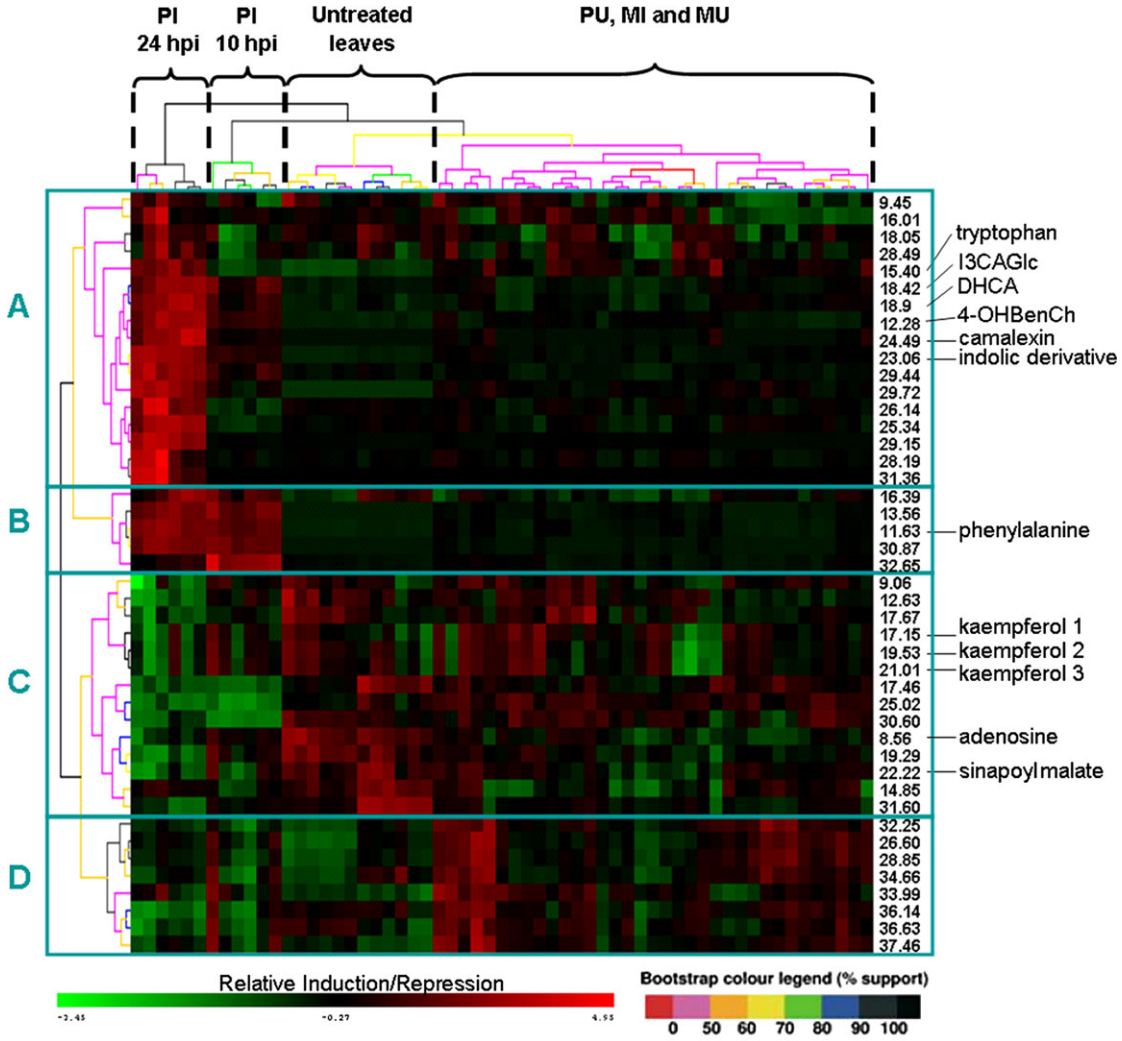

Fig. 4. Major groups of co-regulated secondary metabolites revealed by hierarchical clustering of 44 metabolites and samples issued from different leaf tissues. Data obtained from metabolite profiling of soluble compounds were grouped using average linkage hierarchical clustering with the Pearson correlation coefficient on normalized data. Samples and metabolites were clustered according to their relative induction or repression compared to the median value of all peak areas (green to red colour legend). HCA was made using levels of 44 metabolites from 59 leaf samples. The 44 metabolites are shown horizontally and sorted by their retention time among the clusters A, B, C, and D. The 59 samples shown vertically correspond to two independent experiments. Each experiment groups samples corresponding to untreated leaves, *Pst-AvrRpm1*-infected tissues (PI), the uninfected adjacent part of leaves (PU), mock-infiltrated tissues (MI), and the mock-uninfiltrated adjacent part of leaves (MU). Except for untreated leaves, samples were harvested at 10 hpi or 24 hpi. The tree robustness was determined by bootstrap analysis. Bootstrap values associated with each node are represented by a colour legend shown at the bottom right of the figure. DHCA, dihydrocamalexic acid; 4-OHBenCh, 4-hydroxybenzoylcholine; I3CAGlc, indole-3-carboxylic acid β-D-glucopyranosyl ester; kaempferol 1, kaempferol 3-*O*-[6″-*O*-(rhamnosyl) glucoside] 7-*O*-rhamnoside; kaempferol 2, kaempferol 3-*O*-glucoside 7-*O*-rhamnoside; kaempferol 3, kaempferol 3-*O*-rhamnoside 7-*O*-rhamnoside.

Differential spatial accumulation of SA, camalexin, and scopoletin in Arabidopsis *leaves in response to* Pst-AvrRpm1

Targeted metabolite profiling was performed focusing on SA (Rt 6.01 min), camalexin (Rt 20.02 min) and a compound with an Rt of 17.21 min which was characterized as scopoletin (6-methoxy-7-hydroxycoumarin; *m/z* 193 $[M+H]^+$) by HPLC-MS. Similar low levels of total SA (free and conjugated forms) and free SA were found in untreated and mock-treated leaves. Total SA levels increased in PI tissues reaching 13.02 μg g^{-1} FW 24 hpi (Fig. 6A). In PU tissues, total SA levels showed a lower but significant increase 24 hpi with levels 2-fold higher than in MU tissues and 6-fold lower than in PI tissues. The kinetic pattern of free SA accumulation was similar to that of total SA, but with a 2-fold lower rate. The SA pool was equally distributed between its conjugated forms and its free form in both zones (Fig. 6A, B). Camalexin was neither detected in mock-treated leaves (Fig. 6C) nor in untreated leaves (data not shown), but its accumulation was highly induced in infected tissues 10 hpi and 24 hpi reaching 3.04 and

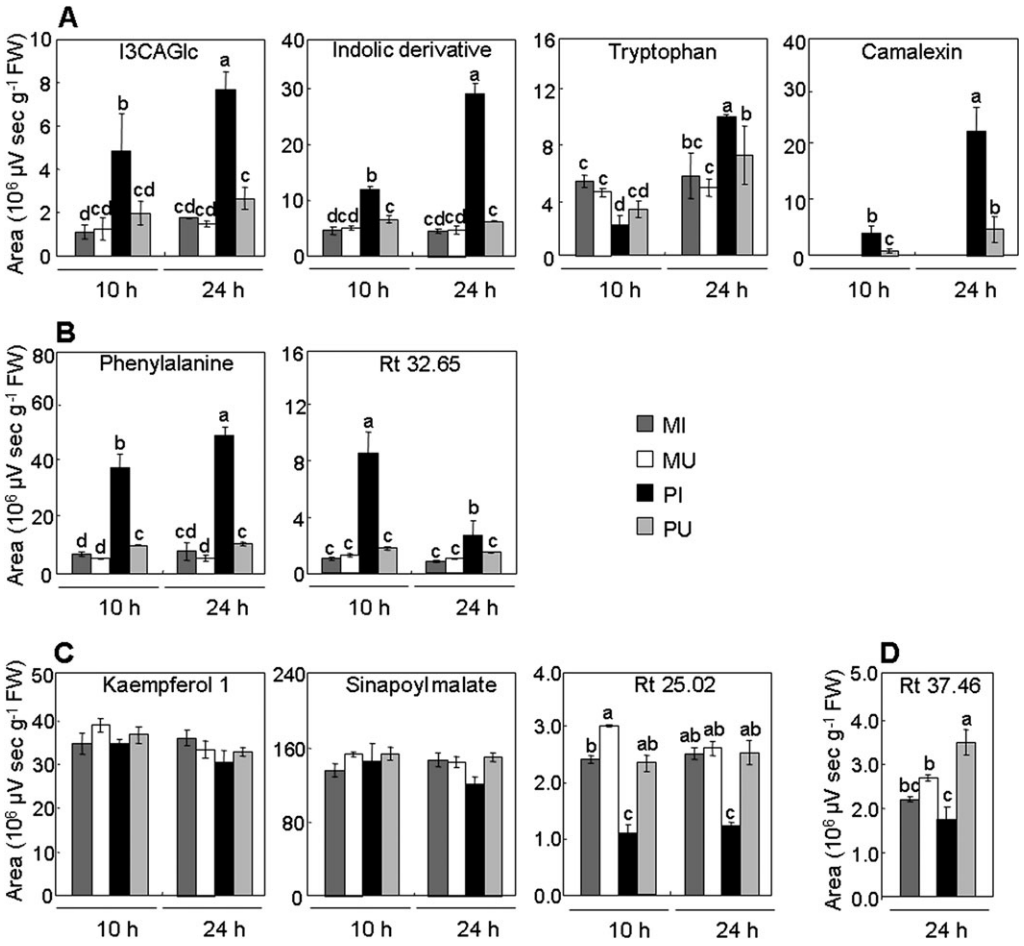

Fig. 5. Relative abundance of secondary metabolites representative of cluster A (A), cluster B (B), cluster C (C), and cluster D (D). Metabolite levels were quantified in *Pst-AvrRpm1*-infected tissues (PI), the uninfected adjacent part of leaves (PU), mock-infiltrated tissues (MI), and the mock-uninfiltrated adjacent part of leaves (MU) at 10 hpi or 24 hpi. Values correspond to the mean and SE of six replicates from two independent experiments. Letters indicate significant differences between values (Newman–Keuls test, P <0.05). In untreated leaves (data not shown), levels of indole-3-carboxylic acid β-D-glucopyranosyl ester (I3CAGlc), the indolic derivative (Rt 23.06 min) and tryptophan reached 1.48±0.14, 3.07±0.29, and 1.95±0.39 10^6 µV s^{-1} g^{-1} FW, respectively; camalexin content was undetectable (cluster A). Levels of phenylalanine and the unknown compound (Rt 32.65) reached 4.51±0.26 and 1.19±0.15 10^6 µV s^{-1} g^{-1} FW respectively (cluster B). Levels of kaempferol 3-*O*-[6″-*O*-(rhamnosyl) glucoside] 7-*O*-rhamnoside (kaempferol 1), sinapoyl malate, and the unknown compound (Rt 25.02) reached 33.80±2.96, 170.37±5.52, and 2.18±0.20 10^6 µV s^{-1} g^{-1} FW, respectively (cluster C). The level of the unknown compound (Rt 37.46) reached 1.44±0.24 10^6 µV s^{-1} g^{-1} FW (cluster D).

6.72 µg g^{-1} FW, respectively (Fig. 6C). Camalexin levels were rather low in PU tissues at 10 hpi, but increased at 24 hpi. Scopoletin and its glucoside scopolin increased in PI and PU tissues (Fig. 6D, E) compared with the mock treatments. Noteworthy, the levels of scopolin, but not of scopoletin, were found to be higher at 24 hpi in PU tissues compared with PI tissues. Treatment of the extracts with β-glucosidase from almond released the same amount of total scopoletin as an acid hydrolysis treatment, indicating that the scopoletin conjugate is the glucoside form, scopolin (data not shown). Scopoletin was not detected in untreated leaves, but scopolin was present in appreciable amounts (0.04 µg g^{-1} FW). Thus, the glucoside was the pre-existing form of the coumarin derivative before infection. Although scopoletin and scopolin accumulated differentially in bacteria-treated leaves, their levels remained quite low compared with SA and camalexin levels. All these results provided direct evidence for a differential quantitative distribution of SA, camalexin, and scopoletin in uninfected and infected part of the same leaf, and may reflect a distinct role for these metabolites during the HR to *Pst-AvrRpm1*.

The occurrence of increased amounts of SA, camalexin, and scopoletin in PU tissues devoid of bacteria raised the question of their site of biosynthesis, either in PI or in PU tissues. To address this question, the expression of *ICS1* (*ISOCHORISMATE SYNTHASE1*), *PAD3* (*PHYTOALEXIN-DEFICIENT3*), and *F6′H1* (*FERULOYL-CoA 6′HYDROXYLASE1*) involved in the biosynthetic pathways of SA, camalexin and scopoletin, respectively, (Wildermuth *et al.*, 2001; Kai *et al.*, 2008; Böttcher *et al.*, 2009) was explored by RT-PCR analysis (Fig. 7). Reverse transcripts of the three genes remained almost undetectable in mock-treated plants. Expression of *ICS1*, *PAD3*, and *F6′;H1* was higher in PI tissues than in PU tissues,

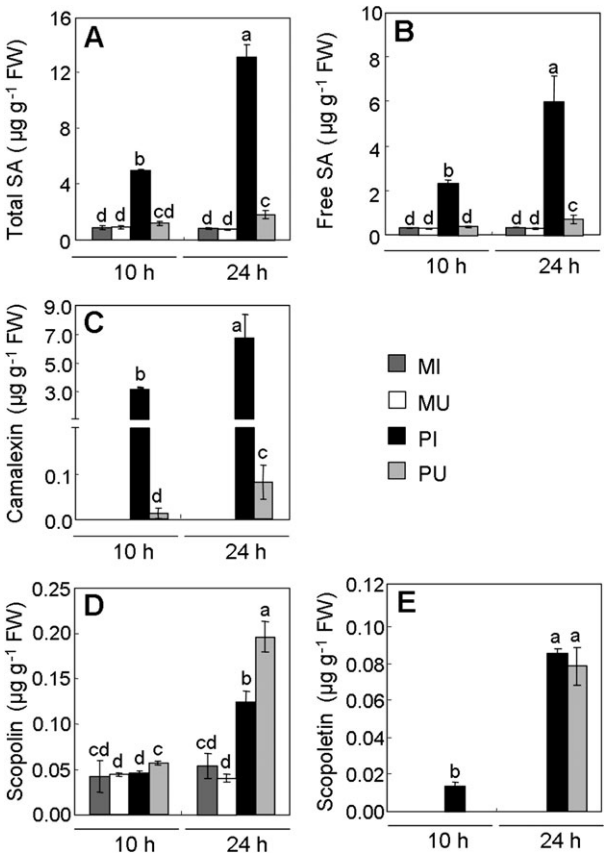

Fig. 6. Quantification of salicylic acid (SA), camalexin, and scopoletin in *Pst-AvrRpm1*-infected tissues (PI), in uninfected adjacent part of leaves (PU), in the mock-infiltrated tissues (MI), and in mock-uninfiltrated adjacent part of leaves (MU) 10 h or 24 h after inoculation. (A) Total pool of SA; (B) free SA; (C) camalexin; (D) scopolin; (E) scopoletin. Values correspond to the mean (±SD) of three replicates from one representative experiment out of two independent experiments. Letters indicate significant differences between values (Newman–Keuls test, P <0.05). In untreated leaves, levels of total SA, free SA, and scopolin reach 1.00±0.11, 0.27±0.02, and 0.04±0.01 µg g^{-1} FW, respectively, while camalexin and scopoletin were undetectable.

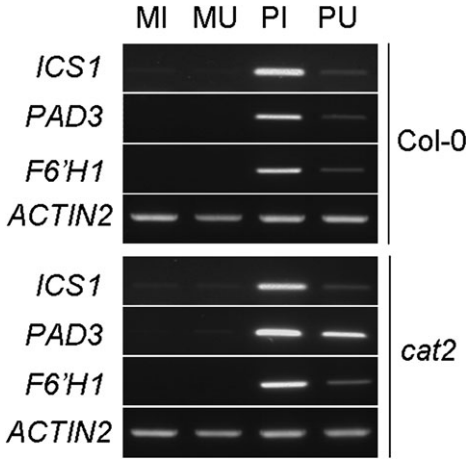

Fig. 7. Expression of *ICS1* (*ISOCHORISMATE SYNTHASE1*), *PAD3* (*PHYTOALEXIN-DEFICIENT3*), and *F6'H1* (*FERULATE-CoA 6'HYDROXYLASE1*) genes in *Pst-AvrRpm1*-treated Col-0 wild-type and *cat2* mutants of *Arabidopsis*. Half leaves of wild-type and *cat2* plants were infiltrated with 10^7 cfu ml^{-1} *Pst-AvrRpm1* or $MgCl_2$. Total RNA was extracted from bacteria-infiltrated (PI) and $MgCl_2$-infiltrated (MI) tissues, from uninfiltrated half leaves of bacteria-treated leaves (PU) and uninfiltrated half leaves of $MgCl_2$-treated leaves (MU). Reverse-transcripts were produced to perform semi-quantitative RT-PCRs. Control reactions to normalize RT-PCR amplification were run with the *ACTIN2* specific primers.

compared with the corresponding mock controls. It strongly suggests that the metabolites present in PU tissues are due to *de novo* synthesis and not to diffusion from PI tissues, although a certain level of diffusion cannot be ruled out.

Metabolic analysis of infected leaves of the cat2 *mutant indicates an enhancement of oxidative burst and cell death correlated with a spatial differential distribution of secondary metabolites*

Because SMs have important interactions with ROS (Chong *et al.*, 1999; Baker *et al.*, 2002; Loreto *et al.*, 2004), their distribution was examined in leaves of CATALASE2-deficient plants (*cat2*) infected with *Pst-AvrRpm1*. The *cat2* mutant shows perturbation of the intracellular redox state but the consequences of this perturbation are further determined by growth conditions (Queval *et al.*, 2007). When grown in long days, the mutant shows activation of a wide range of pathogen responses, suggesting that, in these conditions, *cat2* is a constitutive defence mutant (Chaouch *et al.*, 2010). When grown in short days, however, oxidative stress in *cat2* does not cause constitutive induction of pathogen responses. In this latter growth condition, therefore, *cat2* is a useful model system in which to explore how endogenous oxidative stress interacts with pathogenesis responses triggered by infection.

Accumulation of ROS and cell death were first analysed in the different parts of leaf tissues. Mock-infiltrated wild-type plants and *cat2* mutants did not show any difference in ROS accumulation (Fig. 8A, E, F) and cell death (data not shown). No difference in ROS accumulation and cell death was observed between wild-type and *cat2* untreated plants, confirming that the growth conditions or mock infiltrations do not cause spontaneous formation of lesions in *cat2*. ROS accumulation was next analysed in *cat2* and Col-0 in response to bacterial infection. *cat2* showed a higher accumulation of ROS than wild-type plants in PI tissues at 24 hpi and 48 hpi, and in PU tissues only at 48 hpi (Fig. 8B, C, E, F). PI tissues of wild-type plants exhibited moderate cell death at 24 hpi, while PU tissues did not show any appreciable cell death lesions (Fig. 8D) as MU tissues (data not shown). *cat2* leaves presented more cell death lesions in PI tissues than wild-type leaves at 24 hpi (Fig. 8D) and PU tissues showed only moderate cell death. Non-targeted analysis of soluble compounds in Col-0 and *cat2* mutant infected with *Pst-AvrRpm1* revealed significant differences in the distribution of some SMs, specifically in PI tissues

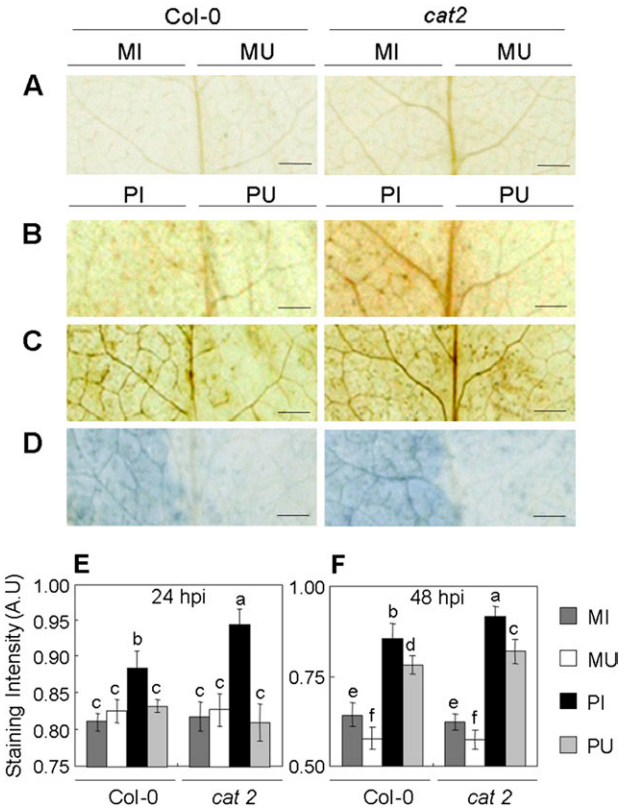

Fig. 8. Reactive oxygen species (ROS) production and cell death detection in *Pst-AvrRpm1*-infected leaves of wild type (Col-0) and *cat2* mutant plants. ROS were detected by DAB staining on whole leaves 24 hpi with $MgCl_2$ (A) or 24 hpi (B) and 48 hpi (C) with *Pst-AvrRpm1*. Cell death was detected by trypan blue staining of whole leaves 24 hpi with *Pst-AvrRpm1* (D). Bars=2 mm. DAB staining intensities at 24 hpi (E) and 48 hpi (F) were quantified using the ImageJ software, for the Col-0 (wild type) and the *cat2* mutant in infected tissues (PI), the uninfected adjacent part of the leaf (PU), mock-infiltrated tissues (MI), the and mock-uninfiltrated adjacent part of the leaf (MU). Values correspond to the mean (±SD) of ten normalized measures from one representative leaf. A total of 12 leaves from two independent experiments was analysed. Letters indicate significant differences between values (Newman–Keuls test, P <0.05).

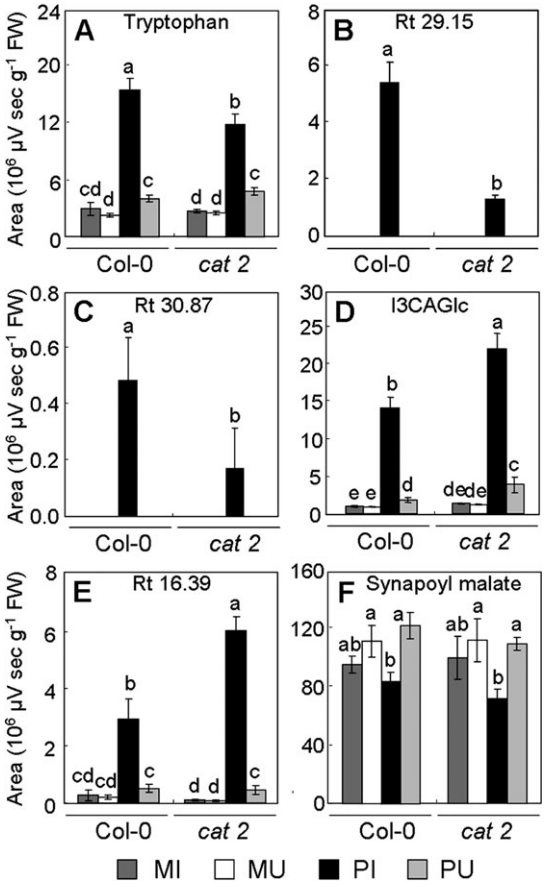

Fig. 9. Relative abundance of compounds differentially induced in Col-0 and *cat2* leaves infected with *Pst-AvrRpm1*. Tryptophan (A), compounds with an Rt of 29.15 min (B) and an Rt of 30.87 min (C) exhibit reduced levels in the *cat2* mutant. Indole-3-carboxylic acid β-D-glucopyranosyl ester (D, I3CAGlc) and the compound with an Rt of 16.39 min (E) exhibit increased levels in the *cat2* mutant. Synapoyl malate (F) exhibits the same levels in the Col-0 wild-type and the *cat2* mutant. Metabolite levels were quantified in *Pst-AvrRpm1*-infected tissues (PI), uninfected adjacent part of leaves (PU), mock-infiltrated tissues (MI), and mock-uninfiltrated adjacent part of leaves (MU) at 24 hpi. Values correspond to the mean (±SD) of three replicates from one experiment. Letters indicate significant differences between values (Newman–Keuls test, P <0.05). In untreated leaves, levels of tryptophan, compounds with an Rt of 29.15 min, a compound with an Rt of 30.87 min, I3CAGlc, the compound with an Rt of 16.39 min, and synapoyl malate reach, respectively, 2.54±1.24, 0.01±0.00, 0.01±0.00, 0.57±0.13, 0.06±0.02, and 108.94±23.20 10^6 µV s g^{-1} FW for Col-0, and 2.68±0.53, 0.01±0.00, 0.01±0.00, 0.90±0.06, 0.09±0.03, and 116.75±25.08 10^6 µV s^{-1} g^{-1} FW for the *cat2* mutant. The experiment was repeated twice with similar results.

(Fig. 9). For example, the accumulation of Trp and unknown compounds with an Rt of 29.15 min and an Rt of 30.87 min were less abundant in PI tissues of *cat2* leaves than in PI tissues of Col-0 leaves (Fig. 9A, B, C). These two latter SMs were not detected in PU tissues. Conversely, I3CAGlc and the compound with Rt 16.39 exhibited a lower level in PI tissues of wild-type plants than in the same corresponding tissues of the *cat2* mutants (Fig. 9D, E). The levels of synapoyl malate (Fig. 9F) and flavonols (data not shown) remained unchanged.

Levels of total SA were the same in Col-0 wild-type and the *cat2* mutant in both zones (Fig. 10A), whereas free SA contents in PI tissues were significantly higher in the *cat2* mutant than in wild-type plants (Fig. 10B). Camalexin accumulation was 1.5-fold less induced in PI tissues of the *cat2* mutant compared with the Col-0 wild type (Fig. 10C), but similar levels were detected in PU tissues. Interestingly, scopolin content was 1.6-fold more abundant in PU tissues of the *cat2* mutants than in PU tissues of the Col-0 wild-type (Fig. 10D). No difference in scopolin levels was observed in PI tissues between *cat2* and wild-type plants. Altogether, these results indicate that disturbance of redox

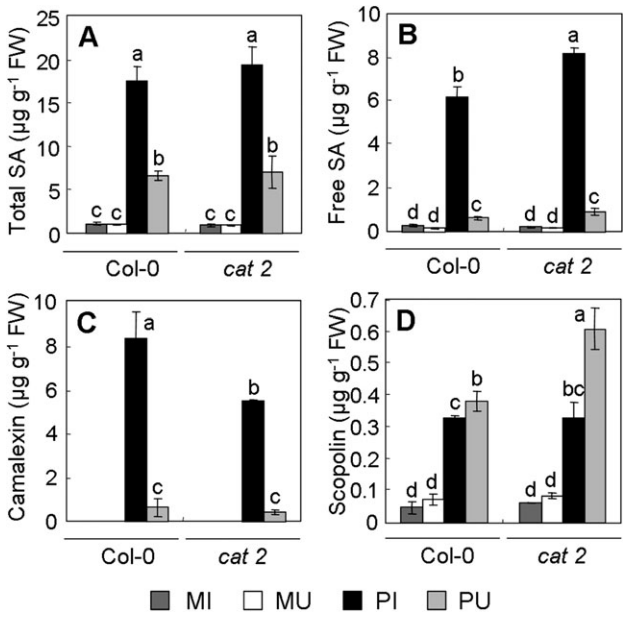

Fig. 10. Quantification of salicylic acid, camalexin, and scopoletin in Col-0 and *cat2 Pst-AvrRpm1*-infected tissues (PI), in the uninfected adjacent part of leaves (PU), in mock-infiltrated tissues (MI), and in mock-uninfiltrated adjacent part of leaves (MU) 24 h after inoculation. (A) Total pool of SA; (B) free SA; (C) camalexin; (D) scopolin. Values correspond to the mean (±SD) of three replicates from one representative experiment out of two independent experiments. Letters indicate significant differences between values (Newman–Keuls test, P <0.05). In untreated leaves, levels of total SA, free SA, and scopolin were 0.94±0.09, 0.20±0.00, and 0.09±0.01 µg g^{-1} FW, respectively, for Col-0, and 1.09±0.07, 0.29±0.04, and 0.06±0.01 µg g^{-1} FW, for the *cat2* mutant; the camalexin content was undetectable.

homeostasis has a quantitative spatial incidence on SM accumulation in infected leaves.

The spatial patterns of *ICS1* and *PAD3* expression in PI and PU tissues (Fig. 7) are similar to those of SA and camalexin accumulation (Fig. 10A, B, C), both in wild-type plants and in the *cat2* mutant. Expression of *F6'H1* did not correlate with scopolin accumulation in PI and PU tissues (Fig. 10D). Expression levels of *PAD3* appeared to be affected in PI and PU tissues of *cat2* mutant compared to wild-type Col-0.

Discussion

Imperfect knowledge of SM distribution in organs or tissues is a key factor limiting the understanding of their biological and ecological role (Wink, 1999). In most plants, synthesis and accumulation of SMs is regulated in space and time (Bednarek and Schulze-Lefert, 2009). Phytoalexins are typically synthesized locally, in proximity to and at the site of pathogen infection (Kuc, 1995). Thus, camalexin was shown to increase mainly in the proximity of lesions of *Arabidopsis* leaves infected with *Botrytis cinerea* (Kliebenstein *et al.*, 2005) while high contents of the indolic derivative were observed at the infection site after infection with *Alternaria alternata* (Schuhegger *et al.*, 2007). Scopoletin, a phytoalexin produced in tobacco leaves infected with TMV or treated with an HR-like elicitor was shown to accumulate preferentially in the surrounding tissues (Chong *et al.*, 2002; Costet *et al.*, 2002). Differential spatial accumulation of the signal metabolite SA occurred between TMV necrotic lesions of tobacco leaves and the neighbouring tissues (Enyedi *et al.*, 1992). Most of the studies concerning the function of SMs are supported by analyses focused on one or two compounds, which is not well suited to give a clear picture of the metabolic organization at the level of a whole tissue or organ. ROS are components of SM differential accumulation at the site of infection during the HR to pathogens and trigger cell death in challenged cells and cellular antioxidant protectant in surrounding cells (Lamb and Dixon, 1997; Dorey *et al.*, 1998; Glawischnig, 2007). Here, both non-targeted and targeted metabolite profiling analyses were performed to decipher the significance of spatial differential distribution of SMs in *Arabidopsis* leaves in relation to H_2O_2 accumulation during the HR to *Pst-AvrRpm1*.

Hierarchical cluster analysis delimits metabolites and metabolic pathways related to their distribution in infected leaves

The spatial differential distribution of SMs was first analysed using metabolite profiling covering the most prominent soluble compounds such as indolics, flavonoids, and phenylpropanoids, which are produced in *Arabidopsis* leaves in response to *Pst-AvrRpm1* infection (Hagemeier *et al.*, 2001; Tan *et al.*, 2003). Non-targeted metabolite profiling of 44 *Pst-AvrRpm1*-inoculated leaf metabolites showed differences between infected and uninfected adjacent tissues which were more quantitative than qualitative (Fig. 3), although some unknown compounds like the metabolite with an Rt of 31.36 min accumulated specifically in PI tissues. Accumulation of this latter compound is either specifically induced in PI tissues or is under the detection threshold in PU tissues. As there is no specific compound typically related to PU tissues, it is tempting to suggest that the secondary metabolism of the uninfected adjacent part of leaf is a subset of that of the infected leaf area.

Positively associated metabolites within the same pathway tend to cluster close together in HCA, while negatively correlated metabolites occupy more distant positions. Hence, four clusters were distinguished. Cluster A groups together late-induced indolic derivatives Fig. 4 which make a great contribution to PI tissue segregation (see Supplementary Fig. S2 at *JXB* online). All major soluble pathogen-induced compounds in *Arabidopsis* leaves were shown to be indolic intermediates or end-products (Hagemeier *et al.*, 2001). Thus, camalexin was especially strongly accumulated in PI tissues (Fig. 4, 5A), a metabolite distribution previously described in

leaves infected with *A. alternata* (Schuhegger *et al.*, 2007). Dihydrocamalexic acid (Rt 18.90 min) exhibited a low accumulation (Fig. 3), indicating a role as an intermediate in camalexin biosynthesis (Schuhegger *et al.*, 2007). The presence of 4-OHBenCh in this cluster is intriguing. This benzoate derivative, although described in low amounts in crucifer leaves (Clausen *et al.*, 1982), accumulated predominantly in *Arabidopsis* seeds of the transparent testa mutant *tt4* affected in flavonoid biosynthesis (Böttcher *et al.*, 2008).

Particularly interesting is cluster B which is represented by Phe and whose components are strongly induced early in PI tissues and barely produced in PU tissues. Phe is at the entry point of phenylpropanoid synthesis and its accumulation may reflect the enhanced incorporation of monolignols into the cell wall (Anterola and Lewis, 2002). Thus, although SA could not be detected in the non-targeted metabolite analyses, its pattern of accumulation (Fig. 6) suggests that it is a typical cluster B compound.

Cluster C groups SMs whose accumulation is not induced or repressed in PI tissues (Fig. 4) like flavonols and sinapoyl malate. Thus, the major part of flavonols in *Arabidopsis* leaves are kaempferol derivatives (Yonekura-Sakakibara *et al.*, 2008) whose levels are not affected either in PI or in PU tissues after *Pst-AvrRpm1* infection. This steady-state level indicates that these flavonoids are not playing any role against the pathogen, but rather are acting as UV-B filters (Winkel-Shirley, 2002). The slight decline in synapoyl malate observed in PI tissues and reported in the same pathosystem (Hagemeier *et al.*, 2001), may be due to the induction of pathogen or plant esterase activity. Adenosine which belongs to cluster C has not been described so far as a metabolite induced in *Arabidopsis-Pst-AvrRpm1* interaction. Bednarek *et al.* (2004) reported the accumulation of 3′-*O*-β-D-ribofuranosyl adenosine exclusively during compatible interaction of *Arabidopsis* with *P. syringae* pv. *tomato*. Moreover, adenosine is a breakdown product of extracellular ATP which was shown to act as a signal potentially in wound and stress response (Song *et al.*, 2006). However, the question here remains open whether adenosine is of bacterial or plant origin or the result of both alternatives together.

Cluster D is certainly the most relevant to PU tissues. Indeed, it is composed of unidentified compounds, such as the metabolite with an Rt of 37.46 min (Fig. 5D; see Supplementary Fig. S3 at *JXB* online), that show antagonistic behaviour in infected and distal tissues, being decreased in PI tissues and induced in PU tissues. However, no SM within this cluster has been identified so far, making it difficult to assign any function to these compounds.

To summarize, it appears that quantitative differences in SM accumulation and distinct metabolic pathways occur within each area of the infected leaf. Tissues engaged in cell death process (PI tissues) are characterized by a highly activated indolic metabolism, while the neighbouring living tissues (PU tissues) are represented by compounds like SMs belonging to cluster D which are certainly those of added value because they are specifically induced in the bordering tissues of the HR sites, and as such could be part of the localized induced resistance (Dorey *et al.*, 1997).

What is the physiological significance of the SA, camalexin, and scopoletin spatial distribution?

Targeted metabolite profiling revealed three major compounds displaying different patterns of accumulation and distribution, namely SA, camalexin, and scopoletin (Fig. 6). SA is a signalling compound in plant defence responses (Shah, 2003), but is also a key player in redox signalling by modulating the activity of NPR1 (Non Expressor of Pathogenesis-Related genes 1), a master regulator of the SA-mediated defence genes (Mou *et al.*, 2003). Although total SA accumulates to high levels in HR tissues, free SA, the active form of SA (Hennig *et al.*, 1993) is induced at low concentrations in the neighbouring tissues (Fig. 6A, B). SA at low doses was shown to prime the activation of defence responses (Shirasu *et al.*, 1997), particularly around the HR lesions as in tobacco leaves reacting hypersensitively to TMV (Mur *et al.*, 1996). Thus, free SA produced in PU tissues at low concentration, could influence the spatial distribution of pathogen priming during the HR to *Pst-AvrRpm1* in *Arabidopsis*.

Camalexin, the major cruciferous indole phytoalexin is induced by a variety of micro-organisms and is synthesized via Trp and indole-3-acetaldoxime in *Arabidopsis* (Glawischnig, 2007; Böttcher *et al.*, 2009). It was shown to accumulate exclusively in the cells of attempted infection and in the close vicinity of lesions (Kliebenstein *et al.*, 2005; Schuhegger *et al.*, 2007). In our model system, camalexin is induced in PI tissues, but also in PU tissues free of bacteria, but to a lesser extent (Fig. 6C). It is noteworthy that camalexin does not contribute to the resistance of *Arabidopsis* to *P. syringae* (Glazebrook and Ausubel, 1994). Thus, the accumulation of camalexin in PI and PU tissues strengthens the conclusion that this indolic compound might have another role without any relationship to resistance, as discussed further below.

Free scopoletin and its glucoside scopolin were identified in *Arabidopsis* inflorescence stems (Rohde *et al.*, 2004), shoots and light-cultivated roots (Bednarek *et al.*, 2005; Kai *et al.*, 2006). Scopoletin was shown to exhibit antimicrobial and antioxidant activities in tobacco (Chong *et al.*, 2002). Here, constitutive levels of scopolin in leaves of *Arabidopsis* are reported (Fig. 6D). The scopolin glucoside pool may serve as a reservoir for delivery of the active free form. Scopolin accumulation is more induced in PU tissues than in PI tissues, 24 h after infection, whereas scopoletin contents remained quite low in both tissues. The differential distribution may be explained by the ROS scavenging capacity of free scopoletin and the stability of scopolin to oxidative stress (Chong *et al.*, 1999). The discrepancy between the weak accumulation of scopoletin/scopolin in *Arabidopsis* leaves undergoing HR and the high levels observed in TMV-infected tobacco leaves (Chong *et al.*, 2002) might reflect species-specificity, a high turn-over rate or a high reactivity of the coumarin derivative to cellular oxidases in *Arabidopsis*.

Whether the overlapping SM distribution patterns observed between PI and PU tissues are the result of a simple diffusion of metabolites from PI tissues or an active process

mediated by signal(s) emanating from PI tissues, or both phenomena operating together, was questioned. Levels of expression of *ICS1*, *PAD3*, and *F'6H1*, the biosynthetic genes involved in SA, camalexin, and scopoletin formation, respectively (Wildermuth *et al.*, 2001; Kai *et al.*, 2008; Böttcher *et al.*, 2009), were clearly higher in PI tissues than in PU tissues (Fig. 7) indicating a likely *de novo* biosynthesis for these SMs. Dorey *et al.* (1997) demonstrated that, in adjacent tissues of tobacco leaf parts infiltrated with a glycoprotein, SA and scopoletin accumulation resulted from *de novo* synthesis rather than from diffusion from infiltrated tissues where HR was occuring.

Oxidative burst is a component of the spatial distribution of secondary metabolites

The distribution and function of SMs in plants attacked by pathogens or herbivores are generally related to resistance and/or signalling (D'Auria and Gershenzon, 2005). Thus, the non-uniform distribution of glucosinolates in *Arabidopsis* appears to explain the feeding preference of herbivore larvae for specific part of leaves (Shroff *et al.*, 2008). However, new roles are emerging for SMs as cellular protectants against oxidative stress (Chong *et al.*, 2002; Gachon *et al.*, 2004). Although a major H_2O_2 source in plant–pathogen interactions is thought to be NADPH-oxidase located in the plasma membrane (Torres *et al.*, 2002), some studies suggest that H_2O_2 produced in the peroxisome may play a role in resistance against disease (Taler *et al.*, 2004). CAT2 is the major isoform detoxifying H_2O_2 generated through peroxisomal photorespiratory activities and plays an indispensable role in preventing redox perturbation (Queval *et al.*, 2007). Therefore, the *cat2* mutant (Queval *et al.*, 2007) is a suitable tool to decipher the link between the production of peroxisomal H_2O_2, the occurrence of cell death, and the distribution of SMs in *Arabidopsis* leaves reacting hypersensitively to *Pst-AvrRpm1*. Production of ROS is more important in PI tissues than in PU tissues in the Col-0 wild-type, whereas cell death is only detectable in PI tissues (Fig. 8). Although constitutively increased ROS are not detectable in *cat2*, the mutant exhibits higher ROS accumulation and a more pronounced cell death in infected leaf tissues than in the adjacent half-part of leaves. This indicates that there is a need for reaching a threshold of ROS accumulation to induce cell death (Van Breusegem and Dat, 2006). Does CAT2 deficiency impact on the distribution of SMs in response to infection? Several of our findings suggest so. It appears first, that the accumulation of Trp and the compounds with Rts of 29.15 min and 30.87 min, is reduced in PI tissues of *cat2* leaves compared with PI tissues of Col-0 wild-type leaves, whereas the accumulation of I3CAGlc and the compound with an Rt of 16.39 is enhanced both in PI and PU tissues (Fig. 9). Two alternatives may explain these different patterns of accumulation. Either these SMs may interact with H_2O_2 and became depleted in *cat2* plants where oxidative stress is higher than in wild-type plants, or signalling and biosynthetic pathways leading to their accumulation may be affected in *cat2*. Second, free SA content was significantly higher in *cat2* PI tissues than in wild-type PI tissues, which did not occur in PU tissues (Fig. 10B). This is consistent with the capability of free SA to be reactive to ROS, and to be distributed in high amounts in tissues undergoing HR where it can play a role in modulating redox balance and protect the leaves from oxidative stress (Yang *et al.*, 2004). Moreover, the spatial pattern of *ICS1* expression (Fig. 7) is similar to total SA accumulation, but not to free SA accumulation (Fig. 10A, B). This indicates that the conjugating activity of SA is not affected by peroxisomal H_2O_2. Third, camalexin content is reduced only in PI tissues of the *cat2* mutant compared with wild-type plants (Fig. 10C). The lower levels of camalexin in HR tissues, despite higher ROS accumulation in infected *cat2*, are surprising because *PAD3* expression appears higher in *cat2* mutants compared with wild-type plants (Fig. 7), and because ROS are important for camalexin induction (Glawischnig, 2007). The depletion of camalexin in PI tissues of the *cat2* mutant may suggest a role for this SM as an antioxidant preventing cell death damage, but without any contribution in resistance against the pathogen. Thus, indole-3-carboxylic acid which is thought to be a cell-wall constituent at infection sites in *Arabidopsis* infected with *Pst-AvrRpm1* (Hagemeier *et al.*, 2001) has been shown to exhibit antioxidant properties (Cano *et al.*, 2003). Fourth, scopolin levels are significantly higher in PU tissues of the *cat2* mutant than in the same tissues of wild-type plants (Fig. 10D), although *F6'H1* expression is similar in wild-type plants and the *cat2* mutant (Fig. 7). The coumarin derivative is derived from the phenylpropanoid pathway through PAL activity, the first committed step of this biosynthetic pathway (Dixon, 2001) and F6'H1 activity (Kai *et al.*, 2008). H_2O_2 was shown to induce *PAL1* gene expression in *Arabidopsis* (Desikan *et al.*, 2001), thus it is possible that accumulation of scopolin in the uninfected-adjacent part of the leaf is sufficient to provide free reactive scopoletin, in combination with other antioxidant SMs, to scavenge the basal level of ROS, as demonstrated during the HR of tobacco leaves infected with TMV (Chong *et al.*, 2002).

Conclusion

Global analysis of SMs at the level of an entire organ without spatial differentiation cannot lead to a true image of the influence and the roles of SMs in the outcome of a plant–pathogen interaction. The distribution of SMs at the site of leaf infection is quantitatively, chemically, and metabolically heterogeneous and redox status appears to be a component of this differential distribution of SMs.

Supplementary data

Supplementary data are available at *JXB* online.

Supplementary Table S1. Secondary metabolite identification based on comparison of HPLC-retention times, PDA-

absorbance spectra, and ESI-MS mass to charge ratio (*m*/*z*) with authentic standards, published data, and data-searches.

Supplementary Fig. S1. Relative abundance of 44 secondary metabolites from $MgCl_2$-infiltrated tissues (MI, black bars) and uninfiltrated adjacent part of leaves (MU, white bars).

Supplementary Fig. S2. Principal Component Analysis of secondary metabolites detected in *Arabidopsis* leaves; score plots (samples).

Supplementary Fig. S3. Principal Component Analysis of secondary metabolites detected in *Arabidopsis* leaves; loading plots (metabolites).

Acknowledgements

We thank Claire Gachon (Scottish Association for Marine Science, Oban, UK) for helpful discussions and comments on the manuscript and Caroline Mauve (Institut de Biologie des Plantes, CNRS-Université Paris-Sud, Orsay, France) for helpful advice. We are grateful to Gilles Comte (CNRS-Université de Lyon 1, Lyon, France) and Dimitri Heintz (Institut de Biologie Moléculaire des Plantes, CNRS, Strasbourg, France) for mass spectra analysis of indolic compounds and scopoletin, respectively. This work was supported by the French Agence Nationale de la Recherche-GENOPLANTE programme 'Sara' (Trilateral 038) and 'Redoxome' (no. GNPO508 G) to FB and ML-M, respectively.

References

Alvarez ME. 2000. Salicylic acid in the machinery of hypersensitive cell death and disease resistance. *Plant Molecular Biology* **44,** 429–442.

Anterola AM, Lewis NG. 2002. Trends in lignin modification: a comprehensive analysis of the effects of genetic manipulations/mutations on lignification and vascular integrity. *Phytochemistry* **61,** 221–294.

Baillieul F, Genetet I, Kopp M, Saindrenan P, Fritig B, Kauffmann S. 1995. A new elicitor of the hypersensitive response in tobacco: a fungal glycoprotein elicits cell death, expression of defence genes, production of salicylic acid, and induction of systemic acquired resistance. *The Plant Journal* **8,** 551–560.

Baker CJ, O'Neill NR, Deahl K, Lydon J. 2002. Continuous production of extracellular antioxidants in suspension cells attenuates the oxidative burst detected in plant microbe interactions. *Plant Physiology and Biochemistry* **40,** 641–644.

Bednarek P, Piślewska-Bednarek M, Svatoš A, *et al*. 2009. A glucosinolate metabolism pathway in living plant cells mediates broad-spectrum antifungal defense. *Science* **323,** 101–106.

Bednarek P, Schneider B, Svatos A, Oldham NJ, Hahlbrock K. 2005. Structural complexity, differential response to infection, and tissue specificity of indolic and phenylpropanoid secondary metabolism in *Arabidopsis* roots. *Plant Physiology* **138,** 1058–1070.

Bednarek P, Schulze-Lefert P. 2009. Role of plant secondary metabolites at the host-pathogen interface. In: Parker J, ed. *Molecular aspect of plant disease resistance*, Vol. 34. Hoboken, USA: Annual Plant Reviews, 220–260.

Bednarek P, Winter J, Hamberger B, Oldham NJ, Schneider B, Tan J, Hahlbrock K. 2004. Induction of 3′- O-β-d-ribofuranosyl adenosine during compatible, but not during incompatible, interactions of *Arabidopsis thaliana* or *Lycopersicon esculentum* with *Pseudomonas syringae* pathovar *tomato*. *Planta* **218,** 668–672.

Böttcher C, von Roepenack-Lahaye E, Schmidt J, Schmotz C, Neumann S, Scheel D, Clemens S. 2008. Metabolome analysis of biosynthetic mutants reveals a diversity of metabolic changes and allows identification of a large number of new compounds in *Arabidopsis*. *Plant Physiology* **138,** 1058–1070.

Böttcher C, Westphal L, Schmotz C, Prade E, Scheel D, Glawischnig E. 2009. The multifunctional enzyme CYP71B15 (PHYTOALAXIN DEFICIENT3) converts cysteine-indole-3-acetonitrile to camalexin in the indole-3-acetonitrile metabolic network of. *Arabidopsis thaliana*. *The Plant Cell* **21,** 1830–1845.

Bowling SA, Clarke JD, Liu Y, Klessig DF, Dong X. 1997. The *cpr5* mutant of *Arabidopsis* expresses both NPR1-dependent and NPR1-independent resistance. *The Plant Cell* **9,** 1573–1584.

Cano A, Alcaraz O, Arnao MB. 2003. Free radical-scavenging activity of indolic compounds in aquaeous and ethanolic media. *Analytical and Bioanalytical Chemistry* **376,** 33–37.

Chaouch S, Queval G, Vanderauwera S, Vandorpe M, Langlois-Meurinne M, Van Breusegem F, Saindrenan P, Noctor G. 2010. Genetic reversion of cell death in the *Arabidopsis cat2* knockout mutant shows that peroxisomal hydrogen peroxide is coupled to biotic defense responses by isochorismate synthase 1 in a daylength-related manner. *Plant Physiology* (in press).

Chong J, Baltz R, Fritig B, Saindrenan P. 1999. An early salicylic acid-, pathogen- and elicitor-inducible tobacco glucosyltransferase: role in compartimentalization of phenolics and H_2O_2 metabolism. *FEBS Letters* **458,** 204–208.

Chong J, Baltz R, Schmitt C, Beffa R, Fritig B, Saindrenan P. 2002. Downregulation of a pathogen-responsive tobacco UDP-Glc:phenylpropanoid glucosyltransferase reduces scopoletin accumulation, enhances oxidative stress, and weakens virus resistance. *The Plant Cell* **14,** 1093–1107.

Clausen S, Olsen O, Sörensen H. 1982. 4-hydroxybenzoylcholine: a natural product present in *Sinapis alba*. *Phytochemistry* **21,** 917–922.

Clay NK, Adio AM, Denoux C, Jander G, Ausubel FM. 2009. Glucosinolate metabolites required for an *Arabidopsis* innate immune response. *Science* **323,** 95–101.

Coleman HD, Park J-Y, Nair R, Chapple C, Mansfield SD. 2008. RNAi-mediated suppression of *p*-coumaroyl-CoA 3′-hydroxylase in hybrid poplar impacts lignin deposition and soluble secondary metabolism. *Proceedings of the National Academy of Sciences, USA* **105,** 4501–4506.

Costet L, Cordelier S, Dorey S, Bailleuil F, Fritig B, Kauffmann S. 1999. Relationship between localized acquired resistance (LAR) and the hypersensitive response (HR): HR is necessary for LAR to

occur and salicylic acid is not sufficient to trigger LAR. *Molecular Plant–Microbe Interactions* **12,** 655–662.

Costet L, Fritig B, Kauffmann S. 2002. Scopoletin expression in elicitor-treated and tobacco mosaic virus-infected tobacco plants. *Physiologia Plantarum* **115,** 228–235.

D'Auria JC, Gershenzon J. 2005. The secondary metabolism of *Arabidopsis thaliana*: growing like a weed. *Current Opinion in Plant Biology* **8,** 308–316.

Desikan R, Mackerness SAH, Hancock JT, Neill SJ. 2001. Regulation of the *Arabidopsis* transcriptome by oxidative stress. *Plant Physiology* **127,** 159–172.

Dixon RA. 2001. Natural products and plant disease resistance. *Nature* **411,** 843–847.

Dorey S, Baillieul F, Pierrel MA, Saindrenan P, Fritig B, Kauffmann S. 1997. Spatial and temporal induction of cell death, defense genes, and accumulation of salicylic acid in tobacco leaves reacting hypersensitively to a fungal glycoprotein elicitor. *Molecular Plant–Microbe Interactions* **10,** 646–655.

Dorey S, Baillieul F, Saindrenan P, Fritig B, Kauffmann S. 1998. Tobacco class I and II catalases are differentially expressed during elicitor-induced hypersensitive cell death and localized acquired resistance. *Molecular Plant–Microbe Interactions* **11,** 1102–1109.

Dutilleul C, Garmier M, Noctor G, Mathieu C, Chétrit P, Foyer CH, de Paepe R. 2003. Leaf mitochondria modulate whole cell redox homeostasis, set antioxidant capacity, and determine stress resistance through altered signaling and diurnal regulation. *The Plant Cell* **15,** 1212–1226.

Enyedi AJ, Yalpani N, Silverman P, Raskin I. 1992. Localization, conjugation, and function of salicylic acid in tobacco during the hypersensitive reaction to tobacco mosaic virus. *Proceedings of the National Academy of Sciences, USA* **89,** 2480–2484.

Foyer CH, Bloom AJ, Queval G, Noctor G. 2009. Photorespiratory metabolism: genes, mutants, energetics, and redox signaling. *Annual Review of Plant Biology* **60,** 455–484.

Gachon CMM, Baltz R, Saindrenan P. 2004. Over-expression of a scopoletin glucosyltransferase in *Nicotiana tabacum* leads to precocious lesion formation during the hypersensitive response to tobacco mosaic virus but does not affect virus resistance. *Plant Molecular Biology* **54,** 137–146.

Gachon CMM, Langlois-Meurinne M, Henry Y, Saindrenan P. 2005. Transcriptional co-regulation of secondary metabolism enzymes in *Arabidopsis*: functional and evolutionary implications. *Plant Molecular Biology* **58,** 229–245.

Glawischnig E. 2007. Camalexin. *Phytochemistry* **68,** 401–406.

Glazebrook J, Ausubel FM. 1994. Isolation of phytoalexin-deficient mutants of *Arabidopsis thaliana* and characterization of their interactions with bacterial pathogens. *Proceedings of the National Academy of Sciences, USA* **91,** 8955–8959.

Hagemeier J, Schneider B, Oldham NJ, Hahlbrock K. 2001. Accumulation of soluble and wall-bound indolic metabolites in *Arabidopsis thaliana* leaves infected with virulent and avirulent *Pseudomonas syringae* pathovar *tomato* strains. *Proceedings of the National Academy of Sciences, USA* **98,** 753–758.

Hahn MG, Bonhoff A, Grisebach H. 1985. Quantitative localization of the phytoalexin glyceollin I in relation to fungal hyphae in soybean roots infected with *Phytophthora megasperma* f. sp. *glycinea*. *Plant Physiology* **77,** 591–601.

Halkier BA, Gershenzon J. 2006. Biology and biochemistry of glucosinolates. *Annual Review of Plant Biology* **57,** 303–333.

Hennig J, Malamy J, Grynkiewicz G, Indulski J, Klessig DF. 1993. Interconversion of the salicylic acid signal and its glucoside in tobacco. *The Plant Journal* **4,** 593–600.

Kai K, Mizutani M, Kawamura N, Yamamoto R, Tamai M, Yamaguchi H, Sakata K, Shimizu B. 2008. Scopoletin is biosynthesized via ortho-hydroxylation of feruloyl CoA by a 2-oxoglutarate-dependent dioxygenase in *Arabidopsis thaliana*. *The Plant Journal* **55,** 989–999.

Kai K, Shimizu B, Mizutani M, Watanabe K, Sakata K. 2006. Accumulation of coumarins in *Arabidopsis thaliana*. *Phytochemistry* **67,** 379–386.

Kliebenstein DJ, Rowe HC, Denby KJ. 2005. Secondary metabolites infuence *Arabidopsis*/ *Botrytis* interactions: variation in host production and pathogen sensitivity. *The Plant Journal* **44,** 25–36.

Kuc J. 1995. Phytoalexins, stress metabolism, and disease resistance in plants. *Annual Review of Phytopathology* **33,** 275–297.

Lamb C, Dixon RA. 1997. The oxidative burst in plant disease resistance. *Annual Review of Plant Physiology and Plant Molecular Biology* **48,** 251–275.

Langlois-Meurinne M, Gachon CMM, Saindrenan P. 2005. Pathogen-responsive expression of glycosyltransferase genes *UGT73B3* and *UGT73B5* is necessary for resistance to *Pseudomonas syringae* pv. *tomato* in *Arabidopsis*. *Plant Physiology* **139,** 1890–1901.

Loake G, Grant M. 2007. Salicylic acid in plant defence: the players and protagonists. *Current Opinion in Plant Biology* **10,** 466–472.

Loreto F, Pinelli P, Manes F, Kollist H. 2004. Impact of ozone on monoterpene emissions and evidence for an isoprene-like antioxidant action of monoterpenes emitted by *Quercus ilex* leaves. *Tree Physiology* **24,** 361–367.

Mou Z, Fan W, Dong X. 2003. Inducers of plant systemic acquired resistance regulate NPR1 function through redox changes. *Cell* **113,** 935–944.

Mur LAJ, Kenton P, Lloyd AJ, Ougham H, Prats E. 2008. The hypersensitive response; the centenary is upon us but how much do we know? *Journal of Experimental Botany* **59,** 501–520.

Mur LAJ, Naylor G, Warner SAJ, Sugars JM, White RF, Draper J. 1996. Salicylic acid potentiates defense gene expression in tissue exhibiting acquired resistance to pathogen attack. *The Plant Journal* **9,** 559–571.

Queval G, Issakidis-Bourguet E, Hoeberichts FA, Vandorpe M, Gakière B, Vanacker H, Miginiac-Maslow M, Breusegem FV, Noctor G. 2007. Conditional oxidative stress responses in the *Arabidopsis* photorespiratory mutant *cat2* demonstrate that redox state is a key modulator of daylength-dependent gene expression, and define photoperiod as a crucial factor in the regulation of H_2O_2-induced cell death. *The Plant Journal* **52,** 640–657.

Rohde A, Morreel K, Ralph J, *et al*. 2004. Molecular phenotyping of the *pal1* and *pal2* mutants of *Arabidopsis thaliana* reveals far-reaching

consequences on phenylpropanoid, amino acid, and carbohydrate metabolism. *The Plant Cell* **16,** 2749–2771.

Saeed A, Sharov V, White J, *et al*. 2003. TM4: a free, open-source system for microarray data management and analysis. *Biotechniques* **24,** 374–378.

Schmelz EA, Engelberth J, Tumlinson JH, Block A, Alborn HT. 2004. The use of vapor phase extraction in metabolic profiling of phytohormones and other metabolites. *The Plant Journal* **39,** 790–818.

Schuhegger R, Rauhut T, Glawischnig E. 2007. Regulatory variability of camalexin biosynthesis. *Journal of Plant Physiology* **164,** 636–644.

Seo S, Seto H, Koshino H, Yoshida S, Ohashi Y. 2003. A diterpene as an endogenous signal for the activation of defense responses to infection with tobacco mosaic virus and wounding in tobacco. *The Plant Cell* **15,** 863–873.

Shah J. 2003. The salicylic acid loop in plant defense. *Current Opinion in Plant Biology* **6,** 365–371.

Shirasu K, Nakajima H, Rajasekhar VK, Dixon RA, Lamb C. 1997. Salicylic acid potentiates an agonist-dependent gain control that amplifies pathogen signals in the activation of defense mechanisms. *The Plant Cell* **9,** 261–270.

Shroff R, Vergara F, Muck A, Svatos A, Gershenzon J. 2008. Nonuniform distribution of glucosinolates in *Arabidopsis thaliana* leaves has important consequences for plant defense. *Proceedings of the National Academy of Sciences, USA* **99,** 517–522.

Song CJ, Steinebrunner I, Wang X, Stout SC, Roux SJ. 2006. Extracellular ATP induces the accumulation of superoxide via NADPH oxidases in *Arabidopsis*. *Plant Physiology* **140,** 1222–1232.

Taler D, Galperin M, Benjamin I, Cohen Y, Kenigsbuch D. 2004. Plant *eR* genes that encode photorespiratory enzymes confer resistance against disease. *The Plant Cell* **16,** 172–184.

Tan J, Bednarek P, Liu J, Schneider B, Svatos A, Hahlbrock K. 2003. Universally occuring phenylpropanoid and species-specific indolic metabolites in infected and uninfected *Arabidopsis thaliana* roots and leaves. *Phytochemistry* **65,** 691–699.

Thomma BPHJ, Nelissen I, Eggermont K, Broekaert WF. 1999. Deficiency in phytoalexin production causes enhanced susceptibility of *Arabidopsis thaliana* to the fungus *Alternaria brassicicola. The Plant Journal* **19,** 163–171.

Torres MA, Dangl JL, Jones JD. 2002. *Arabidopsis* gp91phox homologues AtrbohD and AtrbohF are required for accumulation of reactive oxygen intermediates in the plant defense response. *Proceedings of the National Academy of Sciences, USA* **99,** 517–522.

Van Breusegem F, Dat JF. 2006. Reactive oxygen species in plant cell death. *Plant Physiology* **141,** 384–390.

Wildermuth MC, Dewdney J, Wu G, Ausubel FM. 2001. Isochorismate synthase is required to synthesize salicylic acid for plant defence. *Nature* **417,** 562–565.

Wink M. 1999. Introduction: biochemistry, role and biotechnology of secondary metabolites. In: Wink M, ed. *Functions of plant secondary metabolites and their exploitation in biotechnology*, Vol. 3. Sheffield, UK: Annual Plant Reviews, 1–17.

Winkel-Shirley B. 2002. Biosynthesis of flavonoids and effects of stress. *Current Opinion in Plant Biology* **5,** 218–223.

Yang Y, Qi M, Mei C. 2004. Endogenous salicylic acid protects rice plants from oxidative damage caused by aging as well as biotic and abiotic stress. *The Plant Journal* **40,** 909–919.

Yonekura-Sakakibara K, Tohge T, Matsuda F, Nakabayashi R, Takayama H, Niida R, Watanabe-Takahashi A, Inoue E, Saito K. 2008. Comprehensive flavonol profiling and transcriptome coexpression analysis leading to decoding gene–metabolite correlations in *Arabidopsis*. *The Plant Cell* **20,** 2160–2176.